3.1 Tully-Fisher Distances

• It is an observed phenomenon that spiral galaxies possess a strong correlation between their mean circular velocity v_c and their luminosity L: **Longair, Sec. 2.2**

$$v_c \;=\; 220 \left(\frac{L}{L_*} \right)^{0.22} \;\; \text{km/sec} \;\pm\; 5\% \quad . \tag{10}$$

This is the famous **Tully-Fisher relation** for spirals, first realized in 1977, which exhibits a moderate scatter. Here, the circular velocity is the 3D deprojection of the spectroscopic velocity; i.e. a factor of $\sqrt{3}$ enhancement is invoked. It is usually expressed in terms of absolute magnitudes, which for $10^{10} - 10^{11} M_\odot$ mass spirals naturally falls in the $-18 \to -23$ range. **C & O, pp. 952–5**

Plot: Tully-Fisher Relation for Spirals

$*$ v_c is a measure of the mass $M(r)$ interior to a given radius r by virtue of Kepler's laws: $v_c^2/r = GM(r)/r^2$ ($\Rightarrow M_g \propto v_c^2 r$) for flat rotation curves.

$*$ Note the sequence $M_{Sc} < M_{Sb} < M_{Sa}$ (i.e. $L_{Sa} < L_{Sb} < L_{Sc}$), which is consistent with more light from pronounced spiral arms where massive star formation associated with gas is ongoing.

• The Tully-Fisher relation is naturally expected for *fixed mass-to-light ratios* using the viral theorem, since $L \propto E \propto M_g v_c^2 \propto v_c^4$, where E is the net kinetic energy of the self-gravitating ensemble of stars.

Since $\mathcal{F} = L/(4\pi d^2)$, we can measure $\mathcal{F}$ and infer L using the Tully-Fisher relation and measured v_c. This then yields Tully-Fisher distance estimates:

$$d_{\rm TF} \;\propto\; L^{1/2} \mathcal{F}^{-1/2} \;\propto\; v_c^{9/4}\, \mathcal{F}^{-1/2} \quad , \tag{11}$$

a useful tool in measuring distances to spirals beyond the reach of the Cepheid variable period-luminosity protocol. Then, given $d_{\rm TF}$ and the angular size of a galaxy, we can then infer its radius and hence its mass $M(r) \propto v_c^2 r$, usually to around 10% accuracy.

Tully-Fisher Relation for Spirals

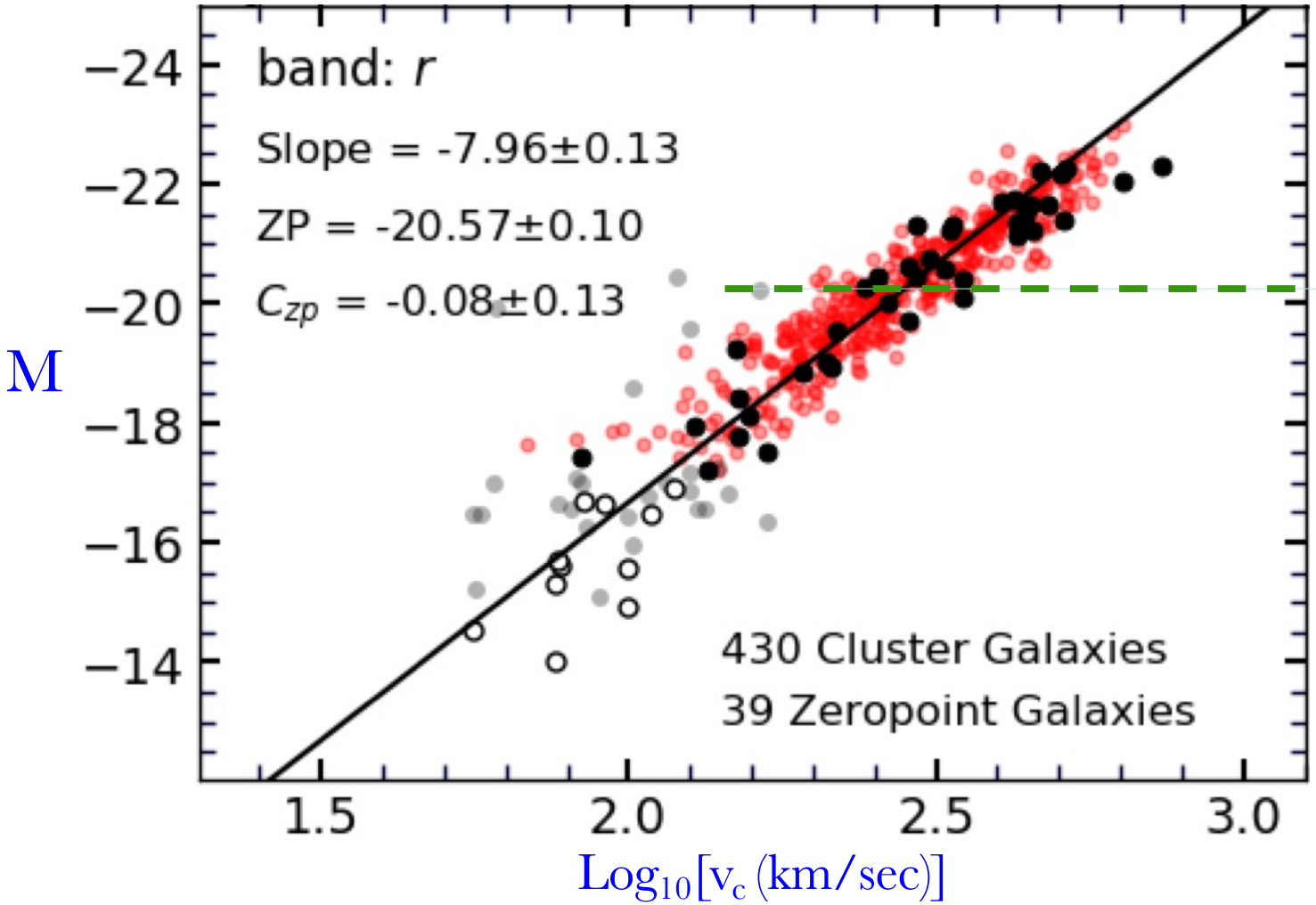

E. Kourkchi et al. (2020, ApJ **896**:3) - Figure 8.

$10^{10} L_{\odot}$

- Tully-Fisher luminosity versus circular velocity v_c map for 430 spiral galaxies in clusters. Uses HI v_c mapping in combination with IR-band brightness information, minimizing dust obscuration. The correlation slope depends modestly on the IR waveband selected.

4 Spiral Structure

• Most majestic spirals, known as **grand-design spirals**, display two prominent, symmetric arms; these are 10% by number. Those like NGC 2841 that do not have well-defined arms, constituting 30% by number are known as **flocculent spirals**. The remaining 60% have multiple arms. **C & O, Sec. 25.3**

• In principal, the arms can have their tips pointing either in or against the direction of galactic rotation; these constitute **leading and trailing spiral arms**, respectively.

Plot: Trailing and Leading Spiral Arm Structure

∗ Doppler shift information in tilted spirals reveals in almost all cases that *spiral arms trail*. This intuitively makes sense: differential rotation in the arms should favor a lag at larger radii where the circular velocity is not $\propto r$.

• Flat rotation curves imply that arms should progressively slip at larger radii, i.e. $\Omega(r)$ is a declining function of r. This would lead to a **winding problem**, where spirals should exhibit many arms after many galactic rotation periods (e.g. like the Parker spiral of the solar wind magnetic field).

Plot: The Spiral Winding Problem

• This conundrum is founded on a purely geometrical picture. In the 1960s, Lin and Shu proposed that spiral arms would constitute self-perpetuating density enhancements through which stars would move and congregate as if in a traffic jam — these are called **spiral density waves**. **C & O, pp. 967–79**

The **Lin-Shu hypothesis** has its origin in **epicyclic** motions of stars about quasi-equilibrium points in rotating frames of reference. The motions are quasi-elliptical in the (R, θ) coordinates, coupled with sinusoidal vertical oscillations in z, and also oscillations in R and θ.

∗ The effective gravitational potential $\Phi_{\rm eff}$ at these equilibrium points is at a local minimum.

Trailing and Leading Spiral Arms

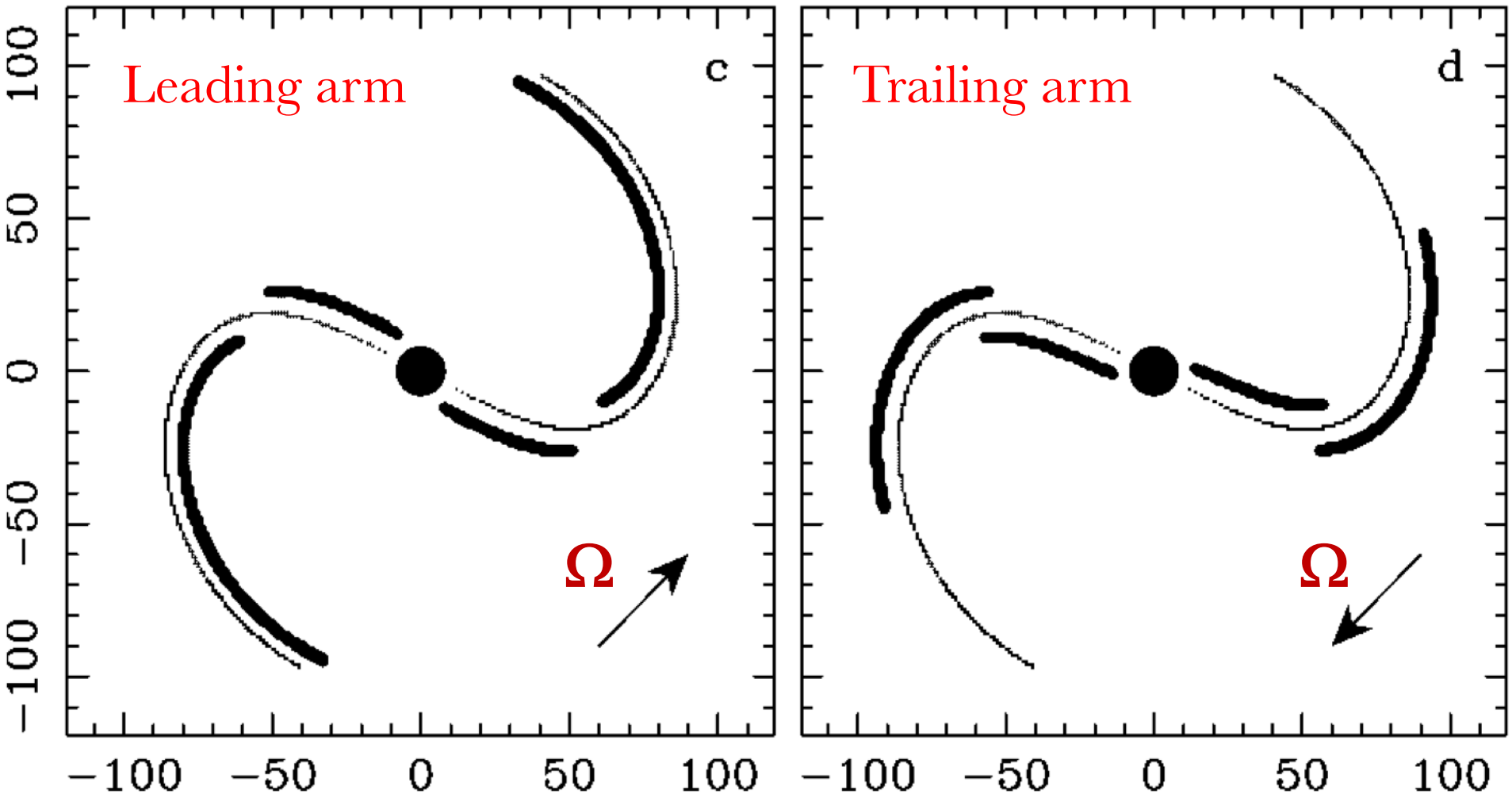

Adapted from Fig. 1 of Puerari & Dottori (ApJ **476**, L73, 1997).

The Spiral Winding Problem

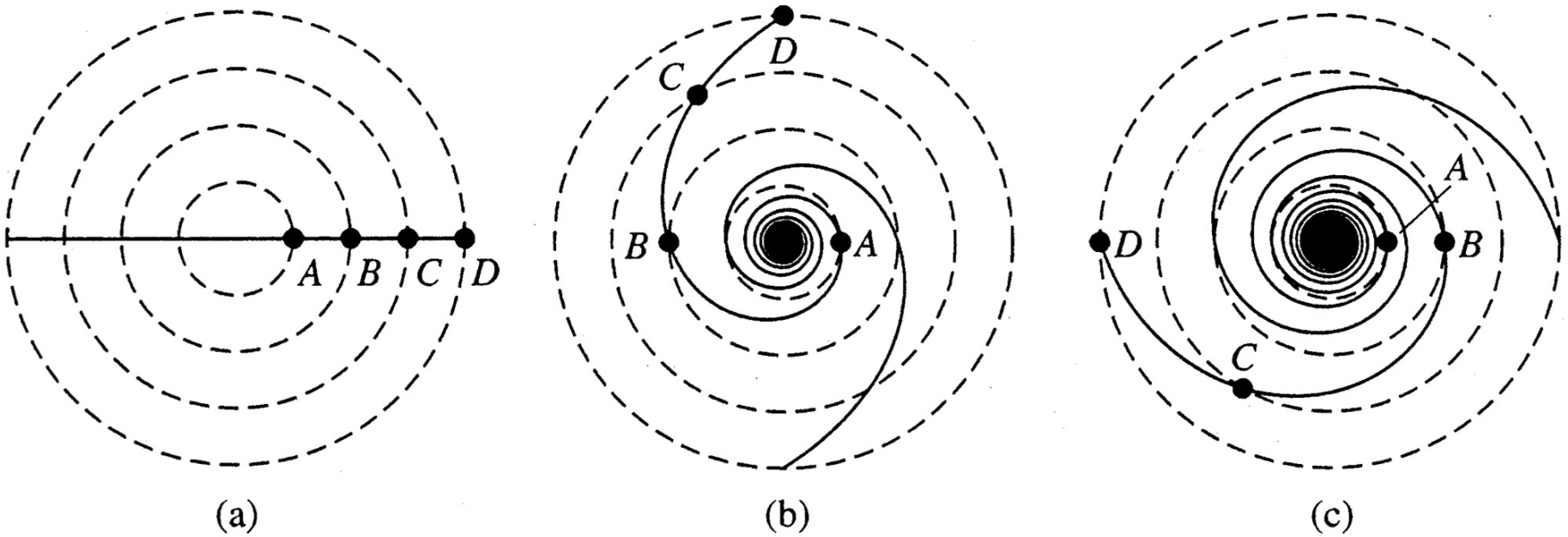

- Progressive temporal snapshots of stars in orbit around a galactic center at the same orbital velocity, so that $\Omega(r) \propto 1/r$. After several galactic rotation periods spiral structure will be tightly wound with many arms.

• This complexity is governed by the equations of motion of stars in the galaxy. Resolving motions into cylindrical coordinates, three components of force emerge. These are

$$\begin{aligned} \ddot{R} - R\dot{\theta}^2 &= -\frac{\partial \Phi}{\partial R} \quad , \quad \text{(radial)} \\ \frac{1}{R}\frac{\partial (R^2\dot{\theta})}{\partial t} &= 0 \quad , \quad \text{(azimuthal)} \\ \ddot{z} &= -\frac{\partial \Phi}{\partial z} \quad . \quad \text{(vertical)} \end{aligned} \tag{12}$$

The azimuthal one expresses a symmetry that translates to a *conservation of angular momentum* (i.e. no net torque) in the vertical direction:

$$R^2\dot{\theta} \;=\; J_z \;=\; \frac{L}{M} \;=\; \text{const.} \tag{13}$$

This integral of the motion can be absorbed into the radial component to modify the equations using an effective gravitational potential for a rotating system (just like Trojan asteroid orbits in the solar system):

$$\Phi_{\text{eff}}(R,\, z) \;\equiv\; \Phi(R,\, z) + \frac{J_z^2}{2R^2} \quad . \tag{14}$$

Combining this with the angular momentum conservation in Eq. (13) yields a radial equation

$$\ddot{R} \;=\; \frac{J_z^2}{R^3} - \frac{\partial \Phi}{\partial R} \;=\; -\frac{\partial \Phi_{\text{eff}}}{\partial R} \quad . \tag{15}$$

Thus, the non-trivial equations of motion then reduce to

$$\ddot{R} \;=\; -\frac{\partial \Phi_{\text{eff}}}{\partial R} \quad , \quad \ddot{z} \;=\; -\frac{\partial \Phi_{\text{eff}}}{\partial z} \quad . \tag{16}$$

A particular star moves in the locale of a local minimum of Φ_{eff} in the R and z dimensions that rotate with the circular velocity $v_c(R)$ of the spiral. A Taylor series expansion of Φ_{eff} about a local minimum yields quadratic terms that guarantee sinusoidal solutions that are perturbed into **epicycles**.

$*$ The approximate vertical symmetry about the galactic plane forces the vertical local minimum to be virtually in the plane.

$*$ To derive a sense of the mathematical character of Φ_{eff}, one can consider the Keplerian case $\Phi = -GM/R$ in Eq. (15), for which $-\partial\Phi/\partial R = GM/R^2$. Then, the equilibrium solution is circular with $J_z^2 = GMR$.

• Two key (virtually independent) frequencies emerge from the sinusoidal solutions of the approximate epicyclic equations: the radial **epicyclic frequency** κ, which applies also to the azimuthal (θ) motion, and the **vertical oscillation** frequency ν.

The timescales of these frequencies can be estimated using fundamental hydrostatics of a self-gravitating stellar ensemble. This naturally establishes $\nu \sim \sqrt{G\rho}$. For a spiral disk with $M \sim 10^{11} M_\odot$ in a cylindrical volume of radius $R \sim 30\,\mathrm{kpc}$ and vertical extent $1\,\mathrm{kpc}$, $\rho \sim 35 M_\odot\,\mathrm{pc}^{-3} \sim 2.4 \times 10^{-21}\,\mathrm{g\ cm}^{-3}$. This yields $\nu \sim 1.3 \times 10^{-14}\,\mathrm{sec}^{-1}$, i.e. an epicyclic period of $2.5\,\mathrm{Myr}$.

• Solutions of particular stellar orbits in the (R, θ) plane are rotating ellipses, and since $\Omega = \Omega(R)$. In the observer frame, these orbits trace out **rosettes** [sketch], and these will be tilted relative to the plane of the sky.

Yet for an ensemble of stars, the average motion at a given R yields elliptical stellar density profiles. In general the orientation of each ellipse of different semi-major axis length is different $\Rightarrow$ **spiral patterns**.

Plot: Nested Ellipses with Twisted Major Axis Configurations

5 Elliptical Galaxies

• Although de Vaucouleurs proposed in 1948 the most commonly-used law for the radial brightness profiles of ellipticals, which we so far have applied to bulges in spirals, an earlier form was proposed in 1930 by Hubble:

$$I(r) \;=\; \frac{I_0}{1 + r^2/a^2} \quad . \tag{17}$$

With the substitution $a = 0.093 r_e$, this compares reasonably well with the de Vaucouleurs profile, except at small and large radii.

Plot: Comparison of Hubble and de Vaucouleurs Profiles

High angular resolution in the optical affords photometric mapping of ellipticals, to generate contour plots of constant intensity (**isophotes**). These trace ellipses, but the projected ellipses' major axes are *not aligned*!

Spiral Density Waves

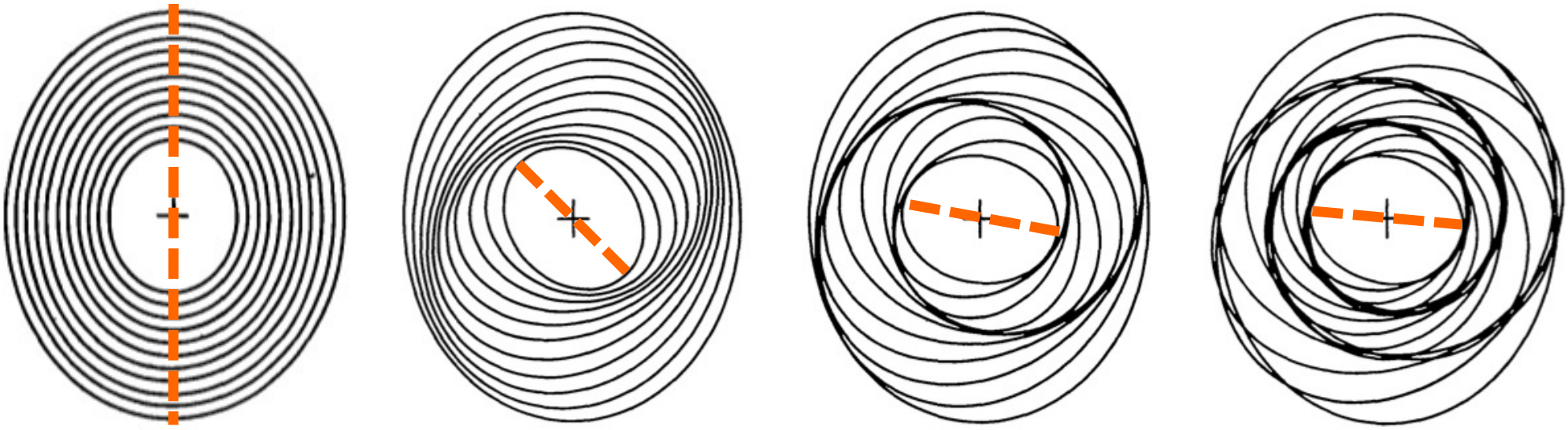

α=0 α=5 α=10 α=16.7

- Precessing elliptical configurations generate spiral waves of enhanced stellar density. The wave morphology is sensitive to the precession "rate" parameter α, where $\theta(a) = -\alpha \log_e a + \text{const}$.
- α =0 gives a bar in the center of the galaxy, also depicted in other panels.
- From Kalnajs, Proc. ASA **2**, 174 (1973).

Hubble's and de Vaucouleurs' Laws

Absolute magnitude

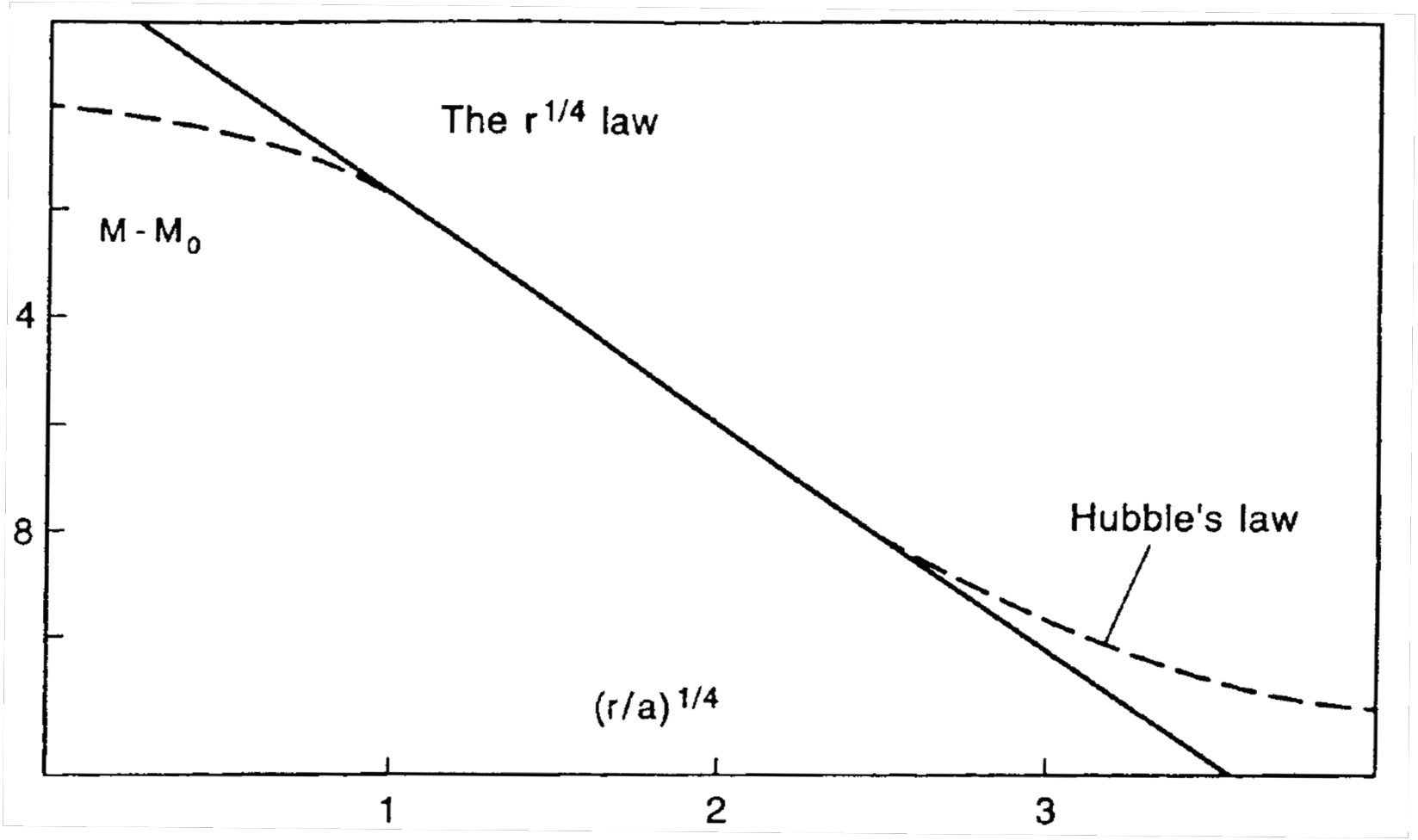

- Comparison of Hubble's $[(r/a) + 1]^{-2}$ profile to de Vaucouleur's $r^{1/4}$ law with $a=0.093\ r_e$. Combes et al. Fig. 1.4.

There is approximate uniform and continuous rotation of isophote contour morphology from the center of many ellipticals. This feature is suggestive evidence for the **triaxial nature** of ellipticals via projection effects.

Plot: Isophote Profile for NGC 4697

$*$ Exceptions to the monotonic trend of isophote axis rotation exist, for example sudden swings in the direction of axis rotation as r is increased. These can provide key indicators of the orientation in space of the ellipsoid.

• The phenomenon of triaxiality, which is not expected in a formation scenario where gravitational collapse conserves angular momentum, could be connected to a proximity of companion galaxies and their tidal influences.

5.1 Populations of Ellipticals

Ellipticals come in a variety of guises, ranging from the comparatively small to the preposterously large. A hitlist of "stars" is as follows:

- **cD galaxies**: immense, but rare. Sometimes as large as 1 Mpc across (more like radio galaxies), and contain masses between $10^{13} - 10^{14} M_\odot$. They have mass-to-light ratios in excess of $300 M_\odot / L_\odot$, implying much dark matter, and can often possess $\gtrsim 10^4$ globular clusters.

- **normal ellipticals**: concentrated brightness in their centers, with a broad range of masses, $10^8 - 10^{13} M_\odot$, and diameters $1 - 200$ kpc. They have mass-to-light ratios in the range $7 - 100 M_\odot / L_\odot$. Lenticulars (S0s and SB0s) are often grouped with normal ellipticals.

- **dwarf ellipticals** (dEs) and **dwarf spheroidals** (dSphs) are usually smaller ($1 - 10$ kpc), less massive ($10^7 - 10^9 M_\odot$), of low surface brightness, and of lower metallicity than normal ellipticals.

- **blue compact dwarf galaxies** (BCDs) are small, but noticeably very blue and with lots of gas. They have many OB stars, and so these galaxies are believed to be undergoing vigorous star formation. They also possess sub-solar mass-to-light ratios $\Rightarrow$ not much dark matter.

Isophotes for Elliptical NGC 4697

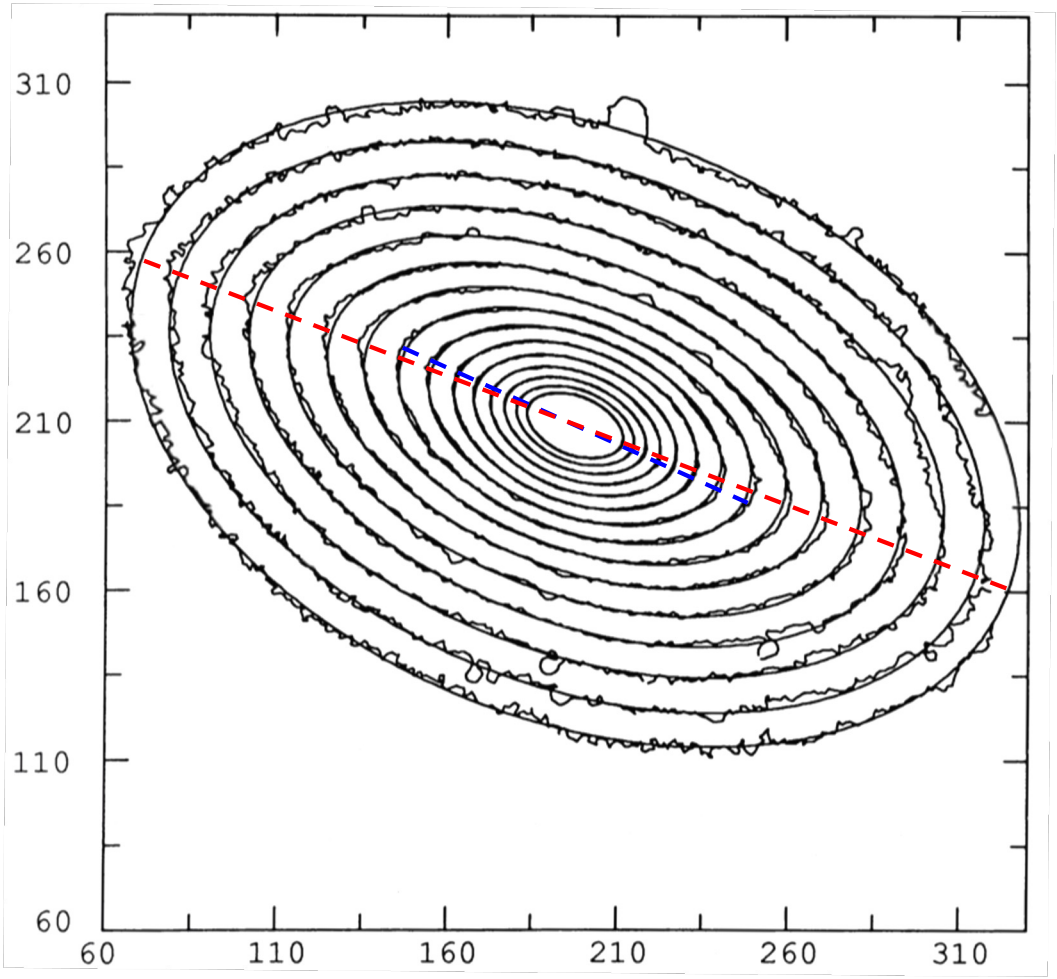

Rotation of ellipse semi-major axes is small for NGC 4697

- Isophotes and ellipse fits for the highly ellipsoidal galaxy NGC 4697 observed by the 4m Anglo-Australian Telescope (AAT). This elliptical displays evidence of a weak disk (~2% by luminosity). Carter, ApJ **312** 514 (1987).